The retention of dust in protoplanetary disks: Evidence from agglomeratic olivine chondrules from the outer Solar System

Devin L. Schrader[1*], Kazuhide Nagashima[2], Scott R. Waitukaitis[3], Jemma Davidson[4], Timothy J. McCoy[5], Harold C. Connolly Jr.[6,7], and Dante S. Lauretta[7].

[1]Center for Meteorite Studies, School of Earth and Space Exploration, Arizona State University, Tempe, AZ 85287-1404, USA.

[2]Hawaiʻi Institute of Geophysics and Planetology, School of Ocean and Earth Science and Technology, University of Hawaiʻi at Mānoa, Honolulu, HI 96822, USA.

[3]Leiden University, Huygens Laboratory, Niels Bohrweg 2, 2333 CA Leiden, Netherlands.

[4]Department of Terrestrial Magnetism, Carnegie Institution of Washington, 5241 Broad Branch Road NW, Washington, District of Columbia 20015–1305, USA.

[5]Department of Mineral Sciences, National Museum of Natural History, Smithsonian Institution, 10th & Constitution Avenue NW, Washington, DC 20560-0119, USA.

[6]Department of Geology, School of Earth & Environment, Rowan University, 201 Mullica Hill Road, Glassboro, NJ 08028, USA.

[7]Lunar and Planetary Laboratory, University of Arizona, Tucson, Arizona 85721, USA.

Geochimica et Cosmochimica Acta,

Volume 223, 15 February 2018, Pages 405–421

Reference:

Schrader D. L., Nagashima K., Waitukaitis S. R., Davidson J., McCoy T. J., Connolly Jr. H. C., and Lauretta D. S. (2018) The retention of dust in protoplanetary disks: Evidence from agglomeratic olivine chondrules from the outer Solar System. *Geochim. Cosmochim. Acta.* **223**, 405–421.

https://doi.org/10.1016/j.gca.2017.12.014

ABSTRACT

By investigating the *in situ* chemical and O-isotope compositions of olivine in lightly sintered dust agglomerates from the early Solar System, we constrain their origins and the retention of dust in the protoplanetary disk. The grain sizes of silicates in these agglomeratic olivine (AO) chondrules indicate that the grain sizes of chondrule precursors in the Renazzo-like carbonaceous (CR) chondrites ranged from <1 to 80 μm. We infer this grain size range to be equivalent to the size range for dust in the early Solar System. AO chondrules may contain, but are not solely composed of, recycled fragments of earlier formed chondrules. They also contain ^{16}O-rich olivine related to amoeboid olivine aggregates and represent the best record of chondrule-precursor materials.

AO chondrules contain one or more large grains, sometimes similar to FeO-poor (type I) and/or FeO-rich (type II) chondrules, while others contain a type II chondrule core. These morphologies are consistent with particle agglomeration by electrostatic charging of grains during collision, a process that may explain solid agglomeration in the protoplanetary disk in the micrometer size regime. The petrographic, isotopic, and chemical compositions of AO chondrules are consistent with chondrule formation by large-scale shocks, bow shocks, and current sheets.

The petrographic, isotopic, and chemical similarities between AO chondrules in CR chondrites and chondrule-like objects from comet 81P/Wild 2 indicate that comets contain AO chondrules. We infer that these AO chondrules likely formed in the inner Solar System and migrated to the comet forming region at least 3 Ma after the formation of the first Solar System solids. Observations made in this study imply that the protoplanetary disk retained a dusty disk at least ~3.7 Ma after the formation of the first Solar System solids, longer than half of the dusty accretion disks observed around other stars.

1.0 INTRODUCTION

The first stage of solid agglomeration in the protoplanetary disk (PPD), which led to the accretion of asteroids, comets, planetesimals, and eventually the rocky planets, involved the collision and capture of individual particles in the nanometer and micrometer size regimes (e.g., Chambers, 2004; Jankowski et al., 2012). These processes of solid agglomeration are likely not unique to the formation of the Solar System, as dusty accretion disks are observed around young stars (e.g., Holland et al., 1998; Meng et al., 2016). Astronomical observations have constrained the lifetime of primordial dusty accretion disks (i.e., not collisional debris disks; Su et al., 2017) around solar-type stars to ≤10 Myr, with only 50% of stars retaining disks beyond an age of ≤1–2 Myr (e.g., Williams and Cieza, 2011). Once the inner accretion disk (R≤0.1 AU) is cleared, the rest of the primordial disk (R≥0.1 to 200 AU) dissipates on a timescale of ~0.5 Myr (e.g., Skrutskie et al., 1990; Williams and Cieza, 2011). From the meteoritic record we know that fine-grained material (i.e., dust) was present during the accretion of asteroids and is present in chondrites as fine-grained matrix. Estimated accretion ages of chondritic parent bodies using thermal modeling (Sugiura and Fujiya, 2014) provides an approximate duration that dusty material was present in the inner Solar System (potentially for the first ~3.6±0.5 Ma of the Solar System; Sugiura and Fujiya, 2014). However, the extent of dusty material and its duration of retention in the PPD is unclear as the residence time of small grains (~20 μm) in the outer Solar System is modeled to be only ~1–2 Myr (Hughes and Armitage, 2010). Therefore, by determining the precursor grain size for age-constrained chondrules thought to have formed in the outer Solar System, we can further constrain the timeframe in which dust was present in the PPD.

The agglomeration of individual particles in the early Solar System led to the formation of chondrules. Chondrules, once partially to fully melted sub-mm to mm-scale objects, are one of the earliest building blocks of asteroids and, eventually, the rocky planets. They are composed primarily of olivine [$(Fe,Mg)_2SiO_4$], pyroxene [$(Fe,Mg,Ca)Si_2O_6$], and plagioclase with minor amounts of Fe,Ni metal, sulfide, and oxide, and are a major component of chondritic meteorites. Chondrules formed from flash heated 'dust balls' in the PPD prior to the accretion of the rocky planets, ~1 to ~3.7 Ma (e.g., Hewins et al., 2005; Kita and Ushikubo, 2012; Schrader et al., 2017; Budde et al., 2018) after the first Solar System solids formed 4567.30±0.16 Ma ago (Connelly et al., 2012). The specific process(es) by which chondrules formed remains undetermined, although numerous models, such as X-wind, solar nebula lightning, impact, current sheets, eccentric planetesimal bow shock, and diskwide gravitational instability shock models have been proposed (e.g., Shu et al., 1996; Desch et al., 2012; Morris et al., 2012; 2016; McNally et al., 2013; Johnson et al., 2015; Dullemond et al., 2016; Krot and Nagashima, 2017). It has been argued that chondrules formed by multiple mechanisms (including shocks, magnetized turbulence, and impacts) within the first 5 Ma of the early Solar System (Krot and Nagashima, 2017).

Chondrules are present in asteroids that likely originated in the inner Solar System (equilibrated LL chondrite-like material, most likely chondrule fragments, were found in samples returned from the S-type asteroid Itokawa; Nakamura et al., 2011), and objects that resemble chondrules are present in a comet that formed in the outer Solar System (comet 81P/Wild 2; Nakamura et al., 2008). This indicates that chondrules formed in the inner Solar System were widely distributed in the PPD (e.g., Nakamura et al., 2008; Brownlee and Joswiak, 2017), and/or that the processes that formed chondrules were wide spread across the PPD (e.g., Van Kooten et al., 2016). However, chondrule-like objects observed in comet 81P/Wild 2 samples recovered by NASA's Stardust sample return mission are often called chondrule-like instead of simply chondrules primarily because of their smaller grain size (e.g., silicate grains typically <10 μm) and wider range in O-isotope compositions compared to typical chondrules (e.g., chondrule-like object Gozen-sama in Nakamura et al. [2008]; Joswiak et al., 2012; Westphal et al., 2017). These objects are chemically and isotopically (O and Al-Mg) most similar to chondrules from the Renazzo-like carbonaceous (CR) chondrites (e.g., Nakashima et al., 2012; 2015; Gainsforth et al., 2015; Ogliore et al., 2012; 2015; Wooden et al., 2017). However, the chemical (Brownlee and Joswiak, 2017) and ^{16}O-rich compositions (Defouilloy et al., 2017) of crystalline silicates from Wild 2 are similar but not identical to silicates in CR chondrite chondrules, and Defouilloy et al. (2017) concluded that Wild 2 pyroxene was most similar to that in amoeboid-olivine-aggregates (AOAs). Additional evidence for a relationship between comet Wild 2 and carbonaceous chondrites include the identification of potential Al-rich chondrules, calcium-aluminum-rich inclusions (CAIs), AOAs, fine-grained matrix-like material, Fe-oxides, and sulfides (e.g., Zolensky et al., 2006; Berger et al., 2011; Bridges et al., 2012; Joswiak et al., 2012, 2014, 2017; Hicks et al., 2017; Nguyen et al., 2017; Westphal et al., 2017).

To constrain chondrule formation conditions and mechanisms, it is essential to determine the compositions of their precursors. Chondrule precursors may include dust clumps, recycled previous generation(s) of chondrules, CAIs, AOAs, and impact debris (melted or unmelted fragments) from differentiated and/or undifferentiated planetesimals (e.g., Jones et al., 2005; Krot et al., 2005; Libourel and Krot, 2007; Connolly and Huss, 2010; Nagashima et al., 2013; Johnson et al., 2015). Regardless of their formation mechanisms, it is generally agreed that chondrule precursors were flash heated to peak temperature for a duration on the order of seconds to minutes, and cooled on the order of hours to days (e.g., Connolly et al., 1998; Hewins et al., 2005; Connolly and Jones, 2016). Chondrules formed from both complete and partial melts, and show petrographic evidence for reheating (e.g., Hewins et al., 2005; Rubin, 2010; Krot and Nagashima, 2017). Some chondrules that were only partially melted during heating retain portions of their solid precursors, termed relict grains (e.g., Jones et al., 2005). The chemical and O-isotope compositions, and morphology of these relict grains provide information about the nature of chondrule precursors.

Chondrules have a range of textures due to distinct peak melting temperatures and cooling rates (e.g., Hewins et al., 2005). Agglomeratic olivine (AO) chondrules were only lightly sintered at peak temperatures <1200°C (Weisberg and Prinz, 1994), the lowest peak temperature of any chondrule type, and therefore retain the vast majority of their precursor silicate materials (e.g., Weisberg and Prinz, 1994, 1996; Ruzicka et al., 2012). Unlike other chondrule types, they are agglomerations of silicates (olivine, pyroxene, and feldspathic glass), oxides, sulfides, and Fe,Ni metal that did not crystalize from a single melt (e.g., Dodd and Van Schmus, 1971; Weisberg and Prinz, 1994, 1996; Ruzicka et al., 2012). These AO chondrules provide information about the grain size and composition of the materials that formed chondrules and eventually accreted to form asteroids and planets. AO chondrules consist of ~57 to 94 vol.% olivine, with a grain size between <1 and 600 µm (Figs. 1 and 2; Weisberg and Prinz, 1994, 1996; Schrader et al., 2013). The majority of chondrules experienced significant to complete melting at peak temperatures of 1400 to 1850ºC (Hewins et al., 2005), and can be classified as type I (FeO-poor; Fe/(Fe + Mg) < 10% atomic ratio) and type II (FeO-rich; Fe/(Fe + Mg) > 10% atomic ratio) chondrules (e.g., Jones et al., 2005). AO chondrules sometimes contain fragments of these chondrule types (Weisberg and Prinz, 1996; Ruzicka et al., 2012). Type I and type II chondrules in the CR chondrites have distinct chemical and O-isotopic compositions (e.g., Krot et al., 2006; Connolly and Huss, 2010; Schrader et al., 2013; 2014; 2017; Tenner et al., 2015), indicating that chondrule fragments in AO chondrules can be identified. It has been proposed that AO chondrules either (1) consist primarily of chondrule precursor materials and minor, rare fragments of earlier formed chondrules (Weisberg and Prinz, 1996) or (2) consist primarily of type I and type II chondrule fragments, and represent a stage of chondrule recycling (Ruzicka et al., 2012).

Due to the high abundance of relict grains in AO chondrules, and similarities between CR chondrite chondrules and chondrule-like objects in comet Wild 2, we studied the chemical and O-isotopic compositions of AO chondrules in the CR chondrites to: (1) determine the origin of their silicate precursors, (2) understand the first stage of solid agglomeration in PPDs through the collision and capture of individual particles, and (3) determine if AO chondrules and chondrule-like objects in comet Wild 2 are related.

2.0 EXPERIMENTAL PROCEDURE

We searched for AO chondrules in 16 CR chondrite polished thin sections; Al Rais USNM1794-8, Elephant Moraine (EET) 87770,31, EET 92048,7, EET 96259,12, Gao-Guenie (b) UA 2301,1, Graves Nunataks (GRA) 95229,22, GRA 06100,26, Grosvenor Mountains 03116,15, LaPaz Ice Field (LAP) 02342,14, LAP 04720,8, Meteorite Hills 00426,33, Northwest Africa 801 UA2300,1, Pecora Escarpment (PCA) 91082,15, Queen Alexandra Range (QUE) 99177,6, Shişr 033 UA2159,1, and Yamato 793495,72-2. A total of eight AO chondrules were identified; one in EET 92048, one in GRA 95229 (Schrader et al., 2013), five in Gao-Guenie (b), and one in PCA 91082. AO chondrules were identified by searching for chondrules dominated by olivine with a typical grain size of <1 to ~10 µm, which may also contain pyroxene, feldspathic glass, oxides, sulfides, and Fe,Ni metal (e.g., Dodd and Van Schmus, 1971; Weisberg and Prinz, 1994, 1996; Ruzicka et al., 2012; Schrader et al., 2013). Olivine in AO chondrules is dominantly FeO-rich, but often contains FeO-poor grains. AO chondrules often do not have well defined boundaries (e.g., Figs. 1 and 2).

2.1 Petrography

An optical microscope was initially used to characterize each thin section. Backscattered electron (BSE) and secondary electron (SE) images were obtained with the dual beam FEI Quanta 3D scanning electron microscope (SEM) at the Open University, the JEOL-8530F electron probe microanalyzer (EPMA) at Arizona State University (ASU), the Cameca SX-100 EPMA at the University of Arizona (UAz), the FEI Nova NanoSEM 600 SEM at the Smithsonian Institution (SI) National Museum of Natural History, Department of Mineral Sciences, and the JEOL Hyperprobe JXA 8500F EPMA and the JEOL JSM-5900LV SEM at the Hawai‘i at Mānoa (UH) (Fig. 1 and Electronic Annex-1 [EA-1]). Apparent chondrule diameters were obtained by measuring the major and minor axes of chondrules using BSE images with Adobe Photoshop® (Table 1 and Figs. 1 and 2).

2.2 Chemical Analyses

Major-element abundances were characterized quantitatively by the Cameca SX-50 and SX-100 EPMAs at UAz, and the JEOL 8900 Superprobe EPMA at SI (Table EA-2). Polished and carbon-coated thin sections were analyzed with a focused beam as individual points, with operating conditions of 15kV and 20 nA, and a ZAF correction method (a Phi-Rho-Z correction technique); peak and background counting times were varied per element to optimize detection limits. Only stoichiometric silicate analyses with totals between 97.0–102.0 wt.% were retained. Standards and detection limits are listed in EA-2.

2.3 O-isotope analyses

Oxygen-isotope compositions were measured with the UH Cameca ims-1280 secondary ion mass spectrometer (SIMS). Olivine grains were measured with an ~20 pA primary beam focused to ~1−2 µm. The secondary ion mass spectrometer was operated at −10 keV with a 40 eV energy window. A normal-incidence electron flood gun was used for charge compensation. Three oxygen isotopes were determined simultaneously: $^{16}O^{-}$, $^{17}O^{-}$, and $^{18}O^{-}$ were measured on a multicollector Faraday Cup (FC) with a 10^{11} ohm resistor, an axial electron multiplier (EM), and a multicollector EM, respectively. The mass resolution for $^{16}O^{-}$ and $^{18}O^{-}$ was ~2000, and that for $^{17}O^{-}$ was ~5700, sufficient to separate interfering $^{16}OH^{-}$. At the end of each analysis, the $^{16}OH^{-}$ signal was monitored, and its contribution to the $^{17}O^{-}$ peak was subtracted. The ^{16}OH contribution to ^{17}O is typically less than 0.2‰ (0.9‰ at most). The grains of interest were marked with a focused electron beam using UH JEOL 5900LV SEM prior to O-isotope measurements so that the marks could be seen in $^{16}O^{-}$ scanning ion image in the ion probe (Nagashima et al., 2015a). After O-isotope analyses, SIMS pits were imaged on the SEM to confirm their locations and to identify if the pits overlap any other phases or cracks (shown in EA-1). The variability of matrix effects in olivine grains with a range of fayalite contents ($Fa_{10–60}$) can result in instrumental mass fractionation (IMF) variations of <2‰ in $\delta^{18}O$ between $Fa_{10–40}$ and 3–4 ‰ between $Fa_{10–60}$ (Jogo et al., 2012); similar to that observed by Ushikubo et al. (2012), Tenner et al. (2015), and Isa et al. (2017). Since IMF is expected to be mass-dependent it should not affect $\Delta^{17}O$. Therefore, $\Delta^{17}O$ is used to compare between FeO-poor and FeO-rich chondrule O-isotope compositions.

Instrumental fractionation was corrected using San Carlos olivine. The external reproducibility of standard measurements (2 standard deviation, 2SD) for $\delta^{17}O$ and $\delta^{18}O$ was ~1.6‰ and ~1.0‰, respectively. Errors represent 2σ analytical uncertainty including both the internal measurement precision (2 standard error of the mean, 2SE) and the external reproducibility (2SD) for standard measurements during a given analytical session (Table 2). Oxygen-isotope compositions are presented as standard delta-notation relative to Standard Mean Ocean Water, $\delta^{17}O_{SMOW}$ and $\delta^{18}O_{SMOW}$, and as deviation from the terrestrial fractionation line, $\Delta^{17}O$ ($\Delta^{17}O = \delta^{17}O_{SMOW} - 0.52 \bullet \delta^{18}O_{SMOW}$).

3.0 RESULTS

3.1 Petrography and chemical compositions

Of the 16 CR chondrite thin sections surveyed, only eight AO chondrules were observed across four thin sections (Figs. 1 and 2). AO chondrules constitute a trace abundance (~0.1 vol.%) of bulk CR chondrites. Type II chondrules make up 2.3% of bulk CR chondrites, or 3.5% of the total chondrule population, while type I chondrules are the most abundant chondrule type at 63.1% of bulk CR chondrites, or 95.8% of the total chondrule population (calculated from Schrader et al., 2011). Four of the eight AO chondrules are solely AO chondrules, the other four contain porphyritic textures identical to type II chondrules. Two of these AO chondrules are compound with porphyritic type II chondrules, while two others consist of a porphyritic olivine pyroxene (POP) texture surrounded by an AO texture (best described as a transitional textured chondrule; labeled AO/type II hereon). The eight AO chondrules range in apparent size from 0.05–1.73 mm (Table 1).

The four compound AO/type II chondrules are EET 92048 AO1, Gao-Guenie (b) Ch14, Ch18, and Ch21. EET 92048 AO1 and Gao-Guenie (b) Ch14 are POP chondrules partially surrounded by AO material (Figs. 1a and 2). The type II portion contains FeO-poor olivine grains, sulfides, and chromite (ideally, $FeCr_2O_4$). However, the AO portion also contains FeO-poor grains and most of the sulfides (pyrrhotite [$(Fe,Ni,Co,Cr)_{1-x}S$] and pentlandite [$(Fe,Ni,Co,Cr)_{9-x}S_8$]). Gao-Guenie (b) Ch18 and Ch21 appear to be porphyritic type II chondrules that are compound with AO chondrules (Figs. 1b,c). The AO portion of Gao-Guenie (b) Ch21 is too fine grained for either reliable *in situ* EPMA or SIMS analyses (mean diameter range for olivine grains, ~1–4 µm). The size of olivine grains in the type II chondrule portions range from ~4–280 µm in mean diameter, while those in the AO portions are smaller, and range from <1 to ~30 µm.

The entirely AO chondrules (i.e., without a type II chondrule portion) are Gao-Guenie (b) Ch21B and Ch22, GRA 95229 Ch15, and PCA 91082 AO1 (Figs. 1c-f; Table 1). Each of these chondrules contains porphyritic olivine in the interiors, but are composed mostly of AO. Gao-Guenie (b) Ch21 and 21B appear to be separate chondrules, but are only separated by ~20 μm of fine-grained matrix (Fig. 1c). PCA 91082 AO1 is an AO chondrule that appears to be deformed or wrapped around an Al-rich chondrule (Fig. 1f). The grain size of olivine in AO chondrules range from <1 to ~30 μm in mean diameter, with the exception of GRA 95229 Ch15 which contains some grains up to 80 μm in mean diameter (Fig. 1e).

The AO chondrules contain FeO-poor ($Fa_{0.8–9.6}$) and FeO-rich olivine ($Fa_{10.9–54.5}$) grains that are normally zoned. The molar Fe/Mn ratio in olivine ranges from 3–116 (Fig. 3, and Table 1 and EA-2). The chemical compositions of olivine within the type II chondrule portion of the compound AO/type II chondrules are identical to that within type II chondrules (Fig. 3 and EA-3) described in Schrader et al. (2015), and so are not discussed here in detail. The chemical compositions of FeO-rich olivine within the AO chondrules and AO portions of AO/type II chondrules are typically indistinguishable from that in type II chondrules (Fig. 3 and EA-3). In contrast, the chemical compositions of FeO-poor olivine in AO chondrules are similar to, but do not have the same compositional range as, type I chondrule olivine; they often have lower abundances of MnO, CaO, and Cr_2O_3 (Fig. 3 and EA-3). No low-iron, manganese enriched (LIME) olivine grains were observed in AO chondrules here. Although some olivine grains have high Mn contents (e.g., 0.96 and 1.13 wt.% MnO; GRA 95229 Ch15 in EA-2), all olivine grains with high MnO contents have FeO > 2 wt.% (the Fe content of LIME olivine is FeO < 2 wt.%; Klöck et al., 1989).

The majority of opaque minerals are sulfides (pentlandite within pyrrhotite), and are typically located along or near the chondrule periphery (Fig. 1). The locations of sulfides are consistent with previous studies of AO chondrules (Weisberg et al., 1994; 1996; Ruzicka et al., 2012). Rare chromite grains are also observed in some AO chondrules (e.g., Figs. 1a and 2), and are more common in type II portions of AO/type II chondrules. Fe,Ni metal was only observed in chondrules PCA 91082 AO1 and EET 92048 AO1 (Fig. 1f and 2). The opaque minerals and their settings in AO chondrules are similar to those of type II chondrules described by Schrader et al. (2015), and so are not described in further detail here.

3.2 Oxygen isotope compositions

The O-isotope compositions of AO chondrules measured here range in $\Delta^{17}O$ from –25±2 to 0±2 ‰, $\delta^{18}O$ from –58±2 to 3±1 ‰, and $\delta^{17}O$ from –56±2 to 0±2 ‰ (2σ; Table 1 and 2 and Figs. 4a and 5a). The O-isotope analyses are distributed near slope-1 lines on the three O-isotope diagram and are mostly ^{16}O-poor (Fig. 4a). The O-isotope composition of each chondrule, except Gao-Guenie (b) Ch21, is heterogeneous in $\Delta^{17}O$ within 2σ uncertainty. We considered a chondrule to be O-isotopically heterogeneous if the $\Delta^{17}O$ of two data points are resolvable within 2σ error (see Table 2). The O-isotope analyses of Gao-Guenie (b) Ch21 (AO/II) are homogeneous within 2σ uncertainty, but analyses were only obtained on olivine in the type II chondrule portion since the AO portion was too fine grained (~1–4 µm in diameter) for *in situ* analyses. O-isotope analyses of fine-grained AO material (both FeO-rich and FeO-poor olivine) are either (1) similar to type I chondrules (e.g., $\Delta^{17}O$= –6.8±0.6 ‰ [Schrader et al., 2013]), (2) similar to type II chondrules (e.g., $\Delta^{17}O$= –0.7±2.1 ‰), or (3) highly ^{16}O-rich (e.g., $\Delta^{17}O$= –25.4±2.0 ‰) (Figures 4a and 5a). The ^{16}O-rich compositions are mostly observed in FeO-poor olivine cores (Fig. 5a). The most FeO-rich olivine with ^{16}O-poor olivine (Gao-Guenie (b) Ch18-5; $\Delta^{17}O$ = –12.0±4.4‰, $Fa_{54.5}$; Table 2) drifted in $\delta^{17}O$ and $\delta^{18}O$ along a slope-1 line during the measurement of this spot, implying the analysis is a mixture of ^{16}O-rich and ^{16}O-poor compositions (Fig. 5a). O-isotope analyses of type II chondrule material are consistent with those of type II chondrules. There is no overall correlation with the Fe content (Fa or Fe#) of the olivine and $\Delta^{17}O$ within AO chondrules (Fig. 5a).

4.0 DISCUSSION

4.1 Chemical, isotopic, and petrographic constraints on chondrule origins

4.1.1. Source of AO chondrule precursors

The chemical and O-isotope compositions of FeO-poor and FeO-rich olivine within AO chondrules indicate multiple sources of chondrule precursors including, but not limited to, type I and type II chondrules (Figs. 3b, 4a, and 5a, and EA-2). The O-isotope compositions of olivine in AO material ($\Delta^{17}O$ = –25.4±2.2 to –0.5±2.1 ‰) overlap with but are sometimes more ^{16}O-rich than type I ($\Delta^{17}O$ = –6.9±2.0 to 0.1±1.1 ‰; Schrader et al., 2013, 2014, 2017) or type II ($\Delta^{17}O$ = –1.8±0.5 to 1.4±0.6 ‰; Schrader et al., 2013, 2014, 2017; Table 2 and Fig. 5a) chondrule phenocrysts. This ^{16}O-rich olivine (e.g., $\Delta^{17}O$ < –20 ‰) in AO chondrules is isotopically inconsistent with an origin from type I or type II chondrule phenocrysts, but is similar to that of refractory inclusions, AOAs and CAIs, in CR chondrites (Fig. 4a). Rare ^{16}O-rich relict olivine grains have been observed in type I and II porphyritic chondrules (e.g., Yurimoto and Wasson, 2002; Jones et al., 2004; Ushikubo et al., 2012), but not in those from the CR chondrites (e.g., Krot et al., 2006; Schrader et al., 2013; 2017; Tenner et al., 2015). This indicates that ^{16}O-rich relict olivine survived in higher abundances in the lightly sintered AO chondrules than in the partially melted (i.e., porphyritic) chondrules. CAIs were the first solid objects to condense in the early Solar System (e.g., Amelin et al., 2002; Bouvier and Wadhwa, 2010; Connelly et al., 2012), and assuming a homogeneous distribution of ^{26}Al in the PPD they formed ~3.7 Ma before CR chondrite chondrules formed (Schrader et al., 2017). AOAs also formed by condensation prior to chondrule formation (Weisberg et al., 2004). CAIs and AOAs have been found within some chondrules (e.g., Krot et al., 2017; Nagashima et al., 2015b). These objects suggest both CAIs and AOAs were present during chondrule formation and therefore may have contributed to chondrule precursors. Olivine is a major component of AOAs, but is rare in CAIs (Aléon et al., 2002; Weisberg et al., 2004). We conclude that the O-isotope compositions of some olivine in AO chondrules are most consistent with, and indicate a relationship to, AOAs. This is similar to the AOA origin for ^{16}O-rich olivine grains in FeO-rich igneous rims around type I chondrules in CR chondrites (i.e., $\Delta^{17}O$ ~ –24 ‰; Nagashima et al., 2013; 2016). Therefore, AO chondrules are not composed solely of recycled type I and type II chondrules. These ^{16}O-rich olivine grain precursors may also suggest that the assumed anhydrous precursor compositions of type I and type II chondrules (e.g., Schrader et al., 2013; Tenner et al., 2015) are too ^{16}O-poor, and should be revised to more AOA-like ^{16}O-rich compositions.

One difference between olivine in AOAs and the AO chondrules studied here is that AOAs in CR chondrites contain LIME olivine (Weisberg et al., 2004), and AO chondrules do not (EA-2). However, this observation does not exclude a genetic relationship. Since the maximum temperature AO chondrules were heated to is <1200°C, their silicates likely underwent solid-state Fe-Mg-Mn diffusion, which is seen in the normal zoning of FeO-poor olivine grains with FeO-rich rims in AO chondrules (Figs. 1 and 2). Since solid-state diffusion rates for Fe, Mg, and Mn are much faster (e.g., Morioka, 1981; Chakraborty, 1997) than O-isotope diffusion in olivine (e.g., Gérard and Jaoul, 1989), Fe-Mg-Mn could homogenize before the O-isotope composition of AO olivine was noticeably altered.

4.1.2. Constraints on AO chondrule formation

The morphologies of AO chondrules suggest that they formed via the agglomeration of <1 to 80 μm diameter silicate grains (see Section 4.2). The AO/type II chondrules likely formed by the agglomeration of such grains around a pre-existing type II chondrule (or type II chondrule fragments; Figs. 1a,b,c and 2). *In situ* chemical and O-isotope analyses confirm that type II chondrule textures in AO/type II chondrules (e.g., $\Delta^{17}O$ = –4.1±1.9 to 0.2±2.0 ‰, 2σ) are consistent with an origin from type II chondrules (e.g., $\Delta^{17}O$ = –4.3±0.7 to 1.4±0.6 ‰, 2σ; Schrader et al., 2013, 2014, 2017; Figs. 4a and 5a and Table 2). AO material almost completely surrounds PO in Gao-Guenie (b) Ch14 (Fig. 1a). This morphology suggests either that (1) the AO material accreted around a pre-existing PO type II chondrule and was reheated (e.g., such as that proposed by Ruzicka et al. 2012), or (2) it is an AO chondrule that was plastically deformed around, and is now compound with, a PO type II chondrule.

The presence of what are most likely type I and II chondrule fragments in some AO chondrules indicates that they formed after/during type I and type II chondrule formation; consistent with the conclusions of Weisberg et al. (1994; 1996) and Ruzicka et al. (2012). Type I and type II chondrules in the CR chondrites, assuming a homogeneous distribution of ^{26}Al, formed contemporaneously between ~2 to >4.5 Ma after the formation of the first Solar System solids (i.e., CAIs), for a mean age of $3.7^{+0.3}_{-0.2}$ Ma or ~3.7 Ma (Nagashima et al., 2014; Schrader et al., 2017). This age is indistinguishable from the CR chondrule age of 3.6±0.6 Ma obtained from Hf-W data (Budde et al., 2018). We suggest the petrographic, isotopic, and compositional data from AO chondrules implies that they formed within or after this time frame.

We conclude that AO chondrules likely contain type I and type II chondrule fragments, as well as ^{16}O-rich precursors related to AOAs. Our results contradict previous work suggesting that AO chondrules consist entirely of recycled chondrules (e.g., Ruzicka et al., 2012), suggesting instead that AO chondrules contain precursor materials, in agreement with Weisberg and Prinz (1994, 1996), which survived because of their lower peak temperatures (i.e., <1200°C; Weisberg and Prinz 1994, 1996; Ruzicka et al., 2012). Therefore, the silicate grain size in AO chondrules indicate that the grain sizes of chondrule precursors in the CR chondrites ranged from <1 to 80 μm; similar to that suggested by Weisberg and Prinz (1996). We infer this grain size range to be equivalent to the size range for dust in the early Solar System. Therefore, we conclude that fine-grained dust was present in the PPD up to at least ~3.7 Ma after the formation of the first Solar System solids. Constraining the grain sizes of chondrule precursor materials that agglomerated into 'dust balls' prior to heating allows us to consider the mechanism(s) for particle agglomeration.

4.2 Agglomeration mechanism of chondrule precursors

The first stage of solid agglomeration in PPDs involves the collision and capture of individual particles in the nanometer and micrometer size regimes. For these particle sizes, sticking arises via minute contact interactions such as van der Waals attraction or liquid bridging via adsorbed surface water. Heim et al. (1999) experimentally determined that for smooth and spherical ~1 μm SiO_2 grains the sticking force is on the order of ~100 nN. Using similar spheres in collision experiments Poppe et al. (2000) found that sticking occurs for impact velocities below ~1 m/s (i.e., a capture energy of ~0.1 fJ over an interaction length of ~1 nm). Given their small size, such grains are in thermal equilibrium with the surrounding gas and consequently have very small (<cm/s) relative velocities (Blum and Wurm, 2008). This implies that growth during this stage is efficient—virtually all collisions lead to capture. For very small aggregates, the sticking force is large enough that rearrangements are difficult and the resulting aggregate structure is fractal (Blum, 2000). As the aggregates become larger, larger impacts unload enough energy to rearrange and compress the aggregates into loosely packed objects

(Blum and Wurm, 2008). Assuming a system initially composed of only these small particles, it is predicted that cm scale "fluffy" aggregates can be formed on a timescale of ~1000 years (Ormel et al, 2007). This timescale is well within the duration of chondrule formation ~0.2–0.4 Ma (i.e., Kita and Ushikubo, 2012), for the majority of chondrules within individual chondrite groups; although full ranges for all chondrules in a group are typically ~0.5–1 Ma (e.g., Kita and Ushikubo, 2012; Nagashima et al., 2014; Schrader et al., 2017).

For perfectly spherical particles, this sticking force (whether from van der Waals or liquid bridging) is predicted to grow with the size*, i.e.,* force is proportional to radius. Royer et al. (2009) used atomic force microscopy to measure the force between larger (~100 µm) silica spheres and found that it is still only on the order of hundreds of nanoNewtons. The discrepancy arises because, at the level of a single contact, the attractive force is not set by the size of the grain, but instead the surface roughness. At this size scale, gravitational attraction is also too weak to cause particles to stick. This suggests that collisions between mm-scale particles should not lead to sticking, however the AO chondrules studied here, and chondrules in general (e.g., Weisberg and Prinz, 1996; Hewins et al., 2005; Ruzikca et al., 2012), provide clear evidence that agglomeration of such particles does occur.

One proposal to resolve this discrepancy is that other forces, specifically electrostatic charging, are at play (Poppe and Schräpler, 2005; Love et al., 2014). The aggregation of particles into dust clumps prior to chondrule formation has been proposed to be electrostatic in nature, and demonstrated through microgravity experiments on the International Space Station (Love et al., 2014). Recent experimental work has verified the counterintuitive result that grains composed of the same material systematically exchange electrical charge during collisions (Waitukaitis and Jaeger, 2013). The mechanism is coupled to differences in particle size, with large particles tending to charge positively and small particles negatively (Waitukaitis et al., 2014). This phenomenon may explain why AO chondrules typically contain one or more relatively large olivine grains (largest grains observed here between 80 and 280 µm; sometimes a type II chondrule core; e.g., Figs. 1a and 2) surrounded by smaller particles (typically <1 to 30 µm) (Figs. 1 and 2b). This creates a negative potential well for an initially neutral system that can trap colliding particles (Lee et al., 2015). Furthermore, a charged grain also creates an attractive force between itself and other uncharged grains through induced polarization (Lee et al., 2015). Though this offers an interesting avenue for continued growth in this size regime, there is currently no knowledge regarding the degree to which this occurs in the PPD. The presence of AO chondrules with size-dependent morphology suggests that such charging processes could have been important for the growth and accretion of chondritic parent bodies after chondrule formation. We further suggest this mechanism may have played a role in the agglomeration of the fine-grained chondritic matrix (<1 μm), potentially nucleating around mm-sized chondrules.

4.3 Implications for models of chondrule formation in the protoplanetary disk

The observation that AO chondrules are composed of chondrule precursor materials of heterogeneous compositions, and not just chondrule fragments, that agglomerated into dust clumps prior to heating allows us to constrain their formation mechanism(s). Currently, the leading debated chondrule formation models include impact into either undifferentiated or differentiated bodies, current sheets, eccentric planetesimal bow shock, and diskwide gravitational instability shock models (e.g., Desch et al., 2012; Morris et al., 2012; 2016; McNally et al., 2013; Johnson et al., 2015; Dullemond et al., 2016).

1) The results of this study are inconsistent with the formation of all chondrules by impact melt droplets due to the collision of early-formed fully differentiated planetesimals. Impact melt formation models have been argued to explain the major, minor, and volatile element composition of chondrules (e.g., Dullemond et al., 2016). However, the O-isotope heterogeneity of AO chondrules cannot be explained by chondrule formation via impact splash between fully differentiated planetesimals. This is because fully differentiated planetesimals have homogenous Δ^{17}O (e.g., Greenwood et al., 2017). Therefore, chondrules formed from impacts would most likely have homogeneous O-isotope compositions. The Δ^{17}O range resulting from the collision between two fully differentiated bodies would be expected to at most be bimodal, which is not observed here. This

observation does not rule out collisions between partially differentiated bodies (i.e., primitive achondrites such as the ureilites), which do retain some O-isotope heterogeneity (e.g., Greenwood et al., 2017).

2) The formation of chondrules by impacts into undifferentiated bodies (e.g., Johnson et al., 2015) does not appear consistent with the results of our study. Impacts into undifferentiated bodies have been invoked to explain the compositional diversity observed in chondrules (Johnson et al., 2015). These impact models are argued to heat heterogeneous material during impact and the material ejected during the collision then cools. However, the formation of AO chondrules by the agglomeration of small (e.g., typically <1 to 30 μm) O-isotopically heterogeneous grains into 'dust clumps' prior to being heated, up to 1200°C, implies these objects were free floating prior to the heating event. Therefore, AO chondrules do not appear consistent with forming during impacts. For example, chondrules from the CB chondrites and some chondrules in the CH chondrites are generally considered have formed in an impact plume resulting from the collision of planetesimals (e.g., Krot and Nagashima, 2017), but these chondrite groups do not contain AO chondrules.
3) The observation that chondrules formed ~1 to ~3.7 Ma (e.g., Hewins et al., 2005; Kita and Ushikubo, 2012; Schrader et al., 2017; Budde et al., 2018) after CAIs is inconsistent with chondrule formation via the X-wind model. Desch et al. (2012) reached this conclusion and discussed that the X-wind model predicts contemporaneous formation of chondrules and CAIs.
4) The implication that AO chondrules formed by the agglomeration of grains into 'dust clumps' prior to being heated, is consistent with chondrule formation in large-scale shocks (e.g., Desch et al., 2012; Morris et al., 2016), bow shocks (e.g., Morris et al., 2012), and current sheets (e.g., McNally et al., 2013). Ruzicka et al. (2012) argued that AO chondrules in unequilibrated ordinary chondrites were consistent with formation in shock waves.

We suggest that the fine-grained material of AO chondrules (e.g., typically <1 to 30 μm) represent the range of dust sizes present in the early Solar System during CR chondrule formation (e.g., ~3.7 Ma after the formation of the first Solar System solids; Nagashima et al., 2014; Schrader et al., 2017; Budde et al., 2018). Therefore, AO chondrules were free floating in the PPD and were then lightly sintered to <1200°C via large-scale shocks, bow shocks, or current sheets.

4.4. Relationship between chondrule-like objects from comet Wild 2 and AO chondrules

AO chondrules are remarkably similar to the chondrule-like objects found in comet Wild 2 samples returned by the Stardust mission. The similarities include their textures, the size of their fine-grained silicates (olivine and pyroxene), the presence of rare chromite (e.g., this study; Nakamura et al. 2008), and the chemical and O-isotope compositions of their olivine (Fig. 5). The silicate minerals in both are unequilibrated and have only been partially melted/lightly sintered, and contain fine-grained ^{16}O-rich FeO-poor olivine with ^{16}O-poor FeO-rich olivine of extremely similar compositions (Figs. 4 and 5). It has been shown that chondrule-like objects from Wild 2 are chemically and isotopically (O and Al-Mg) most similar to chondrules from the CR chondrites (Nakamura et al., 2008; Nakashima et al., 2012; 2015; Gainsforth et al., 2015; Ogliore et al., 2012; 2015), but the minor element compositions of their crystalline silicates are not identical (e.g., Brownlee and Joswiak, 2017; Defouilloy et al., 2017; Fig. 3b). A major difference between chondrule-like objects in Wild 2 and CR type I and type II chondrules is their grain size, with Wild 2 objects being much finer grained than CR type I or type II chondrules (e.g., demonstrated in Figure 5 of Westphal et al., [2017]). In contrast, the grain size of olivine from chondrite-like fragments Torajiro (2 to 5 µm in mean diameter; 7 grains) and Gozen-sama (7 to 14 µm in mean diameter; 2 grains) (measured from images in Nakamura et al., 2008), and Iris (3 to 6 µm in diameter; 5 grains; measured from an image in Ogliore et al., 2012) are similar the grain size of olivine in AO chondrules (<1 to ~30 µm). The abundance of FeO-rich olivine is also distinct between Wild 2 objects and CR chondrules. Type I chondrules are the dominant chondrule type in CR chondrites (e.g., Schrader et al., 2011), but FeO-poor olivine is less common in Wild 2 samples than FeO-rich olivine (e.g., Defouilloy et al., 2017; Westphal et al., 2017).

Another difference is that the most ^{16}O-rich olivine from Wild 2 is also LIME olivine (Nakamura et al., 2008; Nakashima et al., 2015), however no LIME olivine was observed in the AO chondrules studied here. Manganese diffusion due to sintering ~1200°C, as discussed in section 4.1.1 above, may explain this difference and indicate that chondrule-like objects in Wild 2 are less heated than those in CR chondrites. Therefore, CR chondrites and Wild 2 likely did not form from the same reservoir; consistent with the observations of Brownlee and Joswiak (2017) based on differences in the Fe/Mn range of olivine. However, the AO chondrules studied here provide the closest meteoritic analog to the chondrule-like objects from comet Wild 2, and we suggest: (1) they share a similar formation process(es), and (2) the chondrule-like objects in comet Wild 2 are most likely AO chondrules.

The formation regions of both the CR chondrite parent body and of Wild 2 are important to place the similarities of their AO chondrules in context. Comet Wild 2 is a Jupiter Family Comet (JFC) that is thought to have formed at the edge of the solar nebula, was stored beyond the orbit of Neptune (currently ~29.9 to 30.2 AU), and then perturbed into a JFC orbit (Brownlee et al., 2004). In comparison, the CR chondrite parent body formed beyond the snow-line ~4 Ma after the formation of the first Solar System solids (e.g., Sugiura and Fujiya, 2014; Schrader et al., 2017). The CR chondrite parent body may have formed in the outer Solar System beyond the orbit of Jupiter (Warren, 2011) and perhaps Saturn (Van Kooten et al., 2016). The CR chondrite parent body may have then migrated into the inner Solar System due to giant planet migration (e.g., Walsh et al., 2011).

The presence of AO chondrules in both comet Wild 2 and multiple meteorite groups suggest either (1) AO chondrules formed in the inner Solar System (perhaps beyond the orbit of Jupiter, and possibly Saturn), and were distributed to the comet-forming region of the outer Solar System, or (2) they formed in both regions. The low gas density in the outer Solar System led Nakamura et al. (2008) to conclude that radial transport is more likely. However, Van Kooten et al. (2016) argued that chondrules formed in both the inner and outer Solar System. The presence of high temperature phases in comet Wild 2 is also supported by CAIs being found in Wild 2 samples (Zolensky et al., 2006). The observation of abundant high temperature phases in comet Wild 2 samples was generally unexpected, as comets were previously thought to be composed mostly of unprocessed low temperature materials (e.g., Zolensky et al., 2006). If the AO chondrules present in Wild 2 formed in the outer Solar System, it would imply that chondrule formation occurred across the entire PPD (e.g., Van Kooten et al., 2016). If the chondrules did not form in the outer Solar System, it implies that even at >3 Ma after the formation of the first Solar System solids (Ogliore et al., 2012; Nakashima et al., 2015) that objects in the size range of ~10 to ~100 μm (the typical size of AO chondrules observed; Table 1) in the inner Solar System migrated to the outer Solar System. In addition to CAIs and chondrule-like objects, opaque assemblages (i.e., Fe-oxides and sulfides) identified in Wild 2 samples have been argued to have formed in the inner Solar System, and migrated to the comet forming region (e.g., Nguyen et al., 2017). The presence of CAIs in Wild 2 samples demonstrates that migration of some materials occurred, but the presence of AO chondrules may indicate that this migration lasted until at least ~3 Ma (Ogliore et al., 2012; Nakashima et al., 2015) after the formation of the first Solar System solids for Wild 2. To explain the presence of high-temperature phases in comet Wild 2, the migration of material in a viscous disk from the inner Solar System to the outer Solar System was modeled in 2D by Ciesla (2007; 2009), who concluded that the outward migration of material is a natural result of disk formation. Via 1-D disk modeling, Hughes and Armitage (2010) concluded that while particles >1 mm could not be consistently outwardly transported in the PPD, particles in the range of ~20 μm could be radially transported to the outer Solar System. However, the residence time of these small grains in the outer Solar System was modeled to be ~1–2 Myr (Hughes and Armitage, 2010), implying that the accretion of comets occurred within this time frame before the grains migrated back into the inner Solar System (e.g, Hughes and Armitage, 2010; Westphal et al. 2017). Additional evidence for the PPD being well mixed is the inferred homogeneous distribution of ^{26}Al (e.g., Jacobsen et al., 2008; Villeneuve et al., 2009; Schrader et al., 2017) and the uniform distribution of presolar silicon carbide grains across numerous meteorite groups (including CR chondrites) that accreted at different times and heliocentric distances (Davidson et al., 2014). Therefore, we find it more likely that the AO chondrules in Wild 2 formed in the inner Solar System and radially migrated to the outer Solar System. Whether the AO chondrules in Wild 2 formed in the outer

Solar System or in the inner Solar System and migrated to the outer Solar System, their ages (from Ogliore et al., 2012; Nakashima et al., 2015) and presence indicate that the PPD retained a dusty disk in the outer Solar System until at least 3 Ma after the formation of the first Solar System solids.

Our observations do not indicate that AO chondrules from the CR chondrites and comet Wild 2 are the same objects, or formed in the same heating event, radial distance, or time. Our observations also do not indicate that the CR chondrite parent body and comet Wild 2 accreted at the same time. Therefore, our model for the distribution of AO chondrules does not predict the relative abundance of AO chondrules in the CR chondrites vs. comet Wild 2. Our data indicate that AO chondrules in the CR chondrites and comet Wild 2 share petrographic, chemical, and O-isotopic similarities, but there are chemical differences between them. We suggest that these similarities only indicate that both the CR chondrites and comet Wild 2 contain AO chondrules that formed from similar precursor materials under similar formation conditions.

These observations, and the presence of fine-grained matrix in chondrites, imply that the retention of dust in the Solar System persisted from the inner Solar System to the outer Solar System, the entire PPD, until at least ~3.7 Ma, assuming a homogeneous distribution of ^{26}Al. This indicates the dusty disk in our PPD persisted longer than many disks around solar type stars, as only 50% of stars retain a disk beyond an age of $\leq$1–2 Myr (e.g., Williams and Cieza, 2011).

5.0 CONCLUSIONS

1) In the CR chondrites, AO chondrules may contain, but are not solely composed of, recycled type I and type II chondrules. They also contain ^{16}O-rich olivine related to AOAs and represent the best record of chondrule-precursor materials as they experienced lower degrees of thermal processing than other chondrule types.

2) The grain sizes of silicates in AO chondrules indicate that chondrule precursors in the CR chondrites ranged from <1 to 80 µm. We infer this grain size range to be equivalent to the size range for dust in the early Solar System.

3) AO chondrules contain one or more large grains, sometimes similar to type I and/or type II chondrules, while others contain a type II chondrule core. These likely formed by the accretion of fine-grained material around larger grains that were then sintered. These morphologies are consistent with particle agglomeration by electrostatic charging of grains during collision.

4) The petrographic, isotopic, and chemical compositions of AO chondrules are consistent with chondrule formation by large-scale shocks, bow shocks, and current sheets.

5) The petrographic, isotopic, and chemical similarities between AO chondrules and chondrule-like objects from comet Wild 2 indicate that comets contain AO chondrules, and that these AO chondrules likely migrated from the inner Solar System to the comet forming region at least 3 Ma after the formation of the first Solar System solids, with the assumption that ^{26}Al was homogeneously distributed throughout the PPD.

6) Observations made in this study imply that the PPD retained a dusty disk at least ~3.7 Ma after the formation of the first Solar System solids, assuming a homogeneous distribution of ^{26}Al, longer than half of the dusty accretion disks observed around other stars.

Acknowledgements.

For supplying the samples that were necessary for this work, the authors would like to thank: the Smithsonian Institution, the members of the Meteorite Working Group, Cecilia Satterwhite and Kevin Righter (NASA, Johnson Space Center), the National Institute of Polar Research (NIPR), Jack Schrader, and Michael Farmer. US Antarctic meteorite samples are recovered by the Antarctic Search for Meteorites (ANSMET) program, which has been funded by NSF and NASA, and characterized and curated by the Department of Mineral Sciences of the Smithsonian Institution and Astromaterials Curation Office at NASA Johnson Space Center. We thank Diane Johnson and Ian Franchi for the use of, and assistance with, the SEM at the Open University. We are grateful to Tim Gooding and Adam Mansur for assistance with the SEM at SI, Ken Domanik for assistance with EPMA at UA, Axel Wittmann for assistance with EPMA at ASU, and Tim Rose, Emma Bullock, and Steve Lynton for assistance with EPMA at SI. We are also grateful to Daisuke Nakashima, two anonymous reviewers, and Associate Editor Sara Russell, whose constructive comments improved the quality of the manuscript. This research was funded in part by the Arizona State University Center for Meteorite Studies, NASA grant (NNX15AH44H, KN PI), and the Smithsonian Institution.

REFERENCES

Aléon J., Krot A. N., and McKeegan K. D. (2002) Calcium–aluminum-rich inclusions and amoeboid olivine aggregates from the CR carbonaceous chondrites. *Meteorit. Planet. Sci.* **37**, 1729–1755.

Amelin Y., Krot A. N., Hutcheon I. D., and Ulyanov A. A. (2002) Lead isotopic ages of chondrules and calcium–aluminum-rich inclusions. *Science* **297**, 1678–1683.

Berger E. L., Zega T. J., Keller L. P., and Lauretta D. S. (2011) Evidence for aqueous activity on comet 81P/Wild 2 from sulfide mineral assemblages in Stardust samples and CI chondrites. *Geochim. Cosmochim. Acta* **75**, 3501–3513.

Blum J. and Wurm G. (2008) The growth mechanisms of macroscopic bodies in protoplanetary disks. *Annu. Rev. Astro. Astrophys.* **46**, 21–56.

Blum J. (2000) Experiments on sticking, restructuring, and fragmentation of preplanetary dust aggregates. *Icarus* **143**, 138–146.

Brownlee D. E. and Joswiak D. J. (2017) Diversity of the initial rocky planetary building materials at the edge of the solar system. *Meteorit. Planet. Sci.* **52**, 471–478.

Brownlee D. E., Horz F., Newburn R. L., Zolensky M., Duxbury T. C., Sandford S., Sekanina Z., Tsou P., Hanner M. S., Clark B. C., Green S. F., and Kissel J. (2004) Surface of young Jupiter Family Comet 81P/Wild 2: View from the Stardust spacecraft. *Science* **304**, 1764–1769.

Bouvier A. and Wadhwa M. (2010) The age of the Solar System redefined by the oldest Pb–Pb age of a meteoritic inclusion. *Nat. Geosci.* **3**, 637–641.

Bridges J. C., Changela H. G., Nayakshin S., Starkey N. A., and Franchi I. A. (2012) Chondrule fragments from comet Wild2: Evidence for high temperature processing in the outer solar system. *Earth Planet. Sci. Lett.* **341**, 186–194.

Budde G., Kruijer T. S., and Kleine T. (2018) Hf-W chronology of CR chondrites: Implications for the timescales of chondrule formation and the distribution of ^{26}Al in the solar nebula. *Geochim. Cosmochim. Acta* **in press**, https://doi.org/10.1016/j.gca.2017.10.014

Chakraborty S. (1997) Rates and mechanisms of Fe–Mg interdiffusion in olivine at 980–1300°C. *J. Geophys. Res.* **102**, 12317–12331.

Chambers J. E. (2004) Planetary accretion in the inner Solar System. *Earth Planet. Sci. Lett.* **223**, 241–252.

Ciesla F. J. (2007) Outward transport of high-temperature materials around the midplane of the solar nebula. *Science* **318**, 613–615.

Ciesla F. J. (2009) Two-dimensional transport of solids in viscous protoplanetary disks. *Icarus* **200**, 655–671.

Clayton R. N., Onuma N., Grossman L., and Mayeda T. K. (1977) Distribution of the presolar component in Allende and other carbonaceous chondrites. *Earth Planet. Sci. Lett.* **34**, 209–224.

Connelly J. N., Bizzarro M., Krot A. N., Nordlund Å., Wielandt D., and Ivanova M. A. (2012) The absolute chronology and thermal processing of solids in the solar protoplanetary disk. *Science* **338**, 651–655.

Connolly H. C. Jr. and Huss G. R. (2010) Compositional evolution of the protoplanetary disk: Oxygen isotopes of type-II chondrules from CR2 chondrites. *Geochim. Cosmochim. Acta* **74**, 2473–2483.

Connolly H. C. Jr. and Jones R. H. (2016) Chondrules: Canonical and noncanonical views. *Journal of Geophysical Research – Planets* **121**, 1885–1899.

Connolly H. C. Jr., Jones B. D., and Hewins R. H. (1998) The flash melting of chondrules: An experimental investigation into the melting history and physical nature of chondrule precursors. *Geochim. Cosmochim. Acta* **62**, 2725–2735.

Davidson J., Busemann H., Nittler L. R., Alexander C. M. O'D., Orthous-Daunay F.-R., Franchi I. A., and Hoppe P. (2014) Abundances of presolar silicon carbide grains in primitive meteorites determined by NanoSIMS. *Geochim. Cosmochim. Acta* **139**, 248–266.

Defouilloy C., Nakashima D., Joswiak D. J., Brownlee D. E., Tenner T. J., and Kita N. T. (2017) Origin of crystalline silicates from comet 81P/Wild 2: Combined study on their oxygen isotopes and mineral chemistry. *Earth Planet. Sci. Lett.* **465**, 145–154.

Desch S. J. and Connolly H. C. Jr. (2002) A model of the thermal processing of particles in solar nebula shocks: Application to the cooling rates of chondrules. *Meteorit. Planet. Sci.* **37**, 183–207.

Desch S. J., Morris M. A., Connolly H. C., and Boss A. P. (2012) The importance of experiments: Constraints on chondrule formation models. *Meteorit. Planet. Sci.* **47**, 1139–1156.

Dodd R. T. and Van Schmus W. R. (1971) Dark-zoned chondrules. *Chem. Erde* **30**, 49–69.

Dullemond C. P. and Dominik C. (2005) Dust coagulation in protoplanetary disks: A rapid depletion of small grains. *Astron. Astrophys.* **434**, 971–986.

Dullemond C. P., Harsono D., Stammler S. M., and Johansen A. (2016) Forming chondrules in impact splashes II: Volatile retention. *Astrophys. J.* **832**, 91–109.

Frank D. R., Zolensky M. E., and Le L. (2014) Olivine in terminal particles of Stardust aerogel tracks and analogous grain in chondrite matrix. *Geochim. Cosmochim. Acta* **142**, 240–259.

Gainsforth Z., Butterworth A. L., Stodolna J., Westphal A. J., Huss G. R., Nagashima K., Ogliore R., Brownlee D. E., Joswiak D., Tyliszcak T., and Simionovici A. S. (2015) Constraints on the formation environment of two chondrule-like igneous particles from comet 81P/Wild 2. *Meteorit. Planet. Sci.* **50**, 976–1004.

Gérard O. and Jaoul O. (1989) Oxygen diffusion in San Carlos olivine. *J. Geophys. Res.* **94**, 4119-4128.

Greenwood R. C., Burbine T. H., Miller M. F., and Franchi I. A. (2017) Melting and differentiation of early-formed asteroids: The perspective from high precision oxygen isotope studies. *Chemie der Erde - Geochemistry* **77**, 1–43.

Heim L.-O., Blum J., Preuss M., and Butt H.-J. (1999) Adhesion and friction forces between spherical micrometer-sized particles. *Phys. Rev. Lett.* **83**, 3328–3331.

Hewins R. H., Connolly, Jr., H. C., Lofgren G. E., and Libourel G. (2005) Experimental constraints on chondrule formation. In Chondrules and the Protoplanetary Disk (eds. A. N. Krot, E. R. D. Scott and B. Reipurth). ASP Conference Series 341, Astronomical Society of the Pacific, San Francisco. pp. 286–316.

Hicks L. J., MacArthur, Bridges J. C., Price M. C., Wickham-Eade J. E., Burchell M. J., Hansford G. M., Butterworth A. L., Gurman S. J., and Baker S. H. (2017) Magnetite in comet Wild 2: Evidence for parent body aqueous alteration. *Meteorit. Planet. Sci.* **52**, 2075–2096.

Holland W. S., Greaves J. S., Zuckerman B., Webb R. A., McCarthy C., Coulson I. M., Walther D. M., Dent W. R. F., Gear W. K., and Robson I. (1998) Submillimetre images of dusty debris around nearby stars. *Nature* **392**, 788–791.

Hughes A. L. H. and Armitage P. J. (2010) Particle transport in evolving protoplanetary: Implications for results from Stardust. *Astrophys. J.* **719**, 1633–1653.

Isa J., Kohl I. E., Liu M.-C., Wasson J. T., Young E. D., and McKeegan K. D. (2017) Quantification of oxygen isotope SIMS matrix effects in olivine samples: Correlation with sputter rate. *Chem. Geol.* **458**, 14–21.

Jacobsen B., Yin Q.-Z., Moynier F., Amelin Y., Krot A. N., Nagashima K., Hutcheon I. D., and Palme H. (2008) ^{26}Al-^{26}Mg and ^{207}Pb-^{206}Pb systematics of Allende CAIs: Canonical solar initial 26Al/27Al ratio reinstated. *Earth Planet. Sci. Lett.* **272**, 353–364.

Jankowski T., Wurm G., Kelling T., Teiser J., Sabolo W., Gutiérrez P. J., and Bertini I. (2012) Crossing barriers in planetesimal formation: The growth of mm-dust aggregates with large constituent grains. *Astron. Astrophys.* **542**, A80.

Jogo K., Nagashima K., Hutcheon I. D., Krot A. N., and Nakamura T. (2012) Heavily metamorphosed clasts from the CV chondrite breccias Mokoia and Yamato-86009. *Meteorit. Planet. Sci.* **47**, 2251–2268.

Johnson B. C., Minton D. A., Melosh H. J., and Zuber M. T. (2015) Impact getting as the origin of chondrules. *Nature* **517**, 339–341.

Jones R. H., Leshin L. A., Guan Y., Sharp Z. D., Durakiewicz T., and Schilk A. J. (2004) Oxygen isotope heterogeneity in chondrules from the Mokoia CV3 carbonaceous chondrite. *Geochim. Cosmochim. Acta* **68**, 3423–3438.

Jones R. H., Grossman J. N., and Rubin A. E. (2005) Chemical, mineralogical and isotopic properties of chondrules: Clues to their origin. In *Chondrules and the Protoplanetary Disk* (eds. A. N. Krot, E. R. D. Scott and B. Reipurth). ASP Conference Series 341, Astronomical Society of the Pacific, San Francisco. pp. 251–285.

Joswiak D. J., Brownlee D. E., Matrajt G., Westphal A. J., Snead C. J., and Gainsforth Z. (2012) Comprehensive examination of large mineral and rock fragments in Stardust tracks: Mineralogy, analogous extraterrestrial materials, and source regions. *Meteorit. Planet. Sci.* **47**, 471–524.

Joswiak D. J., Nakashima D., Brownlee D. E., Matrajt G., Ushikubo T., Kita N. T., Messenger S., and Ito M. (2014) Terminal particle from Stardust track 130: Probably Al-rich chondrule fragment from comet Wild 2. *Geochim. Cosmochim. Acta* **144**, 277–298.

Joswiak D. J., Brownlee D. E., Nguyen A. N., and Messenger S. (2017) Refractory materials in comet samples. *Meteorit. Planet. Sci.* **47**, 471–524.

Kita N. T. and Ushikubo T. (2012) Evolution of protoplanetary disk inferred from ^{26}Al chronology of individual chondrules. *Meteorit. Planet. Sci.* **47**, 1108–1119.

Klöck W., Thomas K. L., McKay D. S., and Palme H. (1989) Unusual olivine and pyroxene composition in interplanetary dust and unequilibrated ordinary chondrites. *Nature* **339**, 126–128.

Krot A. N. and Nagashima K. (2017) Constraints on mechanisms of chondrule formation from chondrule precursors and chronology of transient heating events in the protoplanetary disk. *Geochem. J.* **51**, 45–68.

Krot A. N., Amelin Y., Cassen P., and Meibom A. (2005) Young chondrules in CB chondrites from a giant impact in the early Solar System. *Nature* **436**, 989–992.

Krot A. N., Libourel G., and Chaussidon M. (2006) Oxygen isotope compositions of chondrules in CR chondrites. *Geochim. Cosmochim. Acta* **70**, 767–779.

Krot A. N., Nagashima K., van Kooten E. M. M., and Bizzarro M. (2017) Calcium-Aluminum-Rich Inclusions Recycled During Formation of Porphyritic Chondrules from CH Carbonaceous Chondrites. *Geochim. Cosmochim. Acta* **201**, 185–223.

Lee V., Waitukaitis S. R., Miskin M. Z., and Jaeger H. M. (2015) Direct observation of particle interactions and clustering in charged granular streams. *Nature Physics* **11**, 733–737.

Libourel G. and Krot A. N. (2007) Evidence for the presence of planetesimal material among the precursors of magnesian chondrules of nebular origin. *Earth Planet. Sci. Lett.* **254**, 1–8.

Love S. G., Pettit D. R., and Messenger S. R. (2014) Particle aggregation in microgravity: Informal experiment on the International Space Station. *Meteorit. Planet. Sci.* **49**, 732–739.

Makide K., Nagashima K., Krot A. N., Huss G. R., Hutcheon I. D., and Bischoff A. (2009) Oxygen- and magnesium-isotope compositions of calcium–aluminum-rich inclusions from CR2 carbonaceous chondrites. *Geochim. Cosmochim. Acta* **73**, 5018–5050.

McKeegan K. D., Kallio A. P. A., Heber V. S., Jarzebinski G., Mao P. H., Coath C. D., Kunihiro T., Wiens R. C., Nordholt J. E., Moses R. W. Jr., Reisenfeld D. B., Jurewicz A. J. G., and Burnett D. S. (2011) The Oxygen Isotopic Composition of the Sun Inferred from Captured Solar Wind. *Science* **332**, 1528–1532.

McNally C. P., Hubbard A., Mac Low M-M., Ebel D. S., and D'Alessio P. (2013) Mineral processing by short circuits in protoplanetary disks. *Astrophys. J. Lett.* **767**, L2.

Meng H. Y. A., Plavchan P., Rieke G. H., Cody A. M., Güth T., Stauffer J., Covey K., Carey S., Ciardi D., Duran-Rojas M. C., Gutermuth R. A., Morales-Calderón M., Rebull L. M., and Watson A. M. (2016) Photo-reverberation mapping of a protoplanetary accretion disk around a T Tauri Star. *Astrophys. J.* **823**, 58–72.

Morioka M. (1981) Cation diffusion in olivine – II. Ni-Mg, Mn-Mg, Mg and Ca. *Geochim. Cosmochim. Acta* **45**, 1573–1580.

Morris M. A., Boley A. C., Desch S. J., and Athanassiadou T. (2012) Chondrule formation in bow shocks around eccentric planetary embryos. *Astrophys. J.* **752**, 27.

Morris M. A., Weidenschilling S. J., and Desch S. J. (2016) The effect of multiple particle sizes on cooling rates of chondrules produced in large-scale shocks in the solar nebula. *Meteorit. Planet. Sci.* **51**, 870–883.

Nagashima N., Krot A. N., Libourel G., and Huss G. R. (2013) Magnesian porphyritic chondrules surrounded by ferroan igneous rims from CR chondrite GRA 95229. *Lunar Planet. Sci.* XLIV, Lunar Planet. Inst., Houston, #1780.

Nagashima K., Krot A. N., and Huss G. R. (2014) ^{26}Al in chondrules from CR2 chondrites. *Geochem. J.* **48**, 561–570.

Nagashima K., Krot A. N., and Huss G. R. (2015a) Oxygen-isotope compositions of chondrule phenocrysts and matrix grains in Kakangari K-grouplet chondrite: Implication to a chondrule-matrix genetic relationship. *Geochim. Cosmochim. Acta* **151**, 49–67.

Nagashima K., Krot A. N., and Park C. (2015b) An Amoeboid Olivine Aggregate Surrounded by an Igneous Ferroan Olivine-Rich Rim from CO3.0 Chondrite DOM 08006. *Lunar Planet. Sci.* XLVI, Lunar Planet. Inst., Houston, #2477.

Nagashima N., Krot A. N., Libourel G., and Schrader D. L. (2016) ^{16}O-rich olivine abundances in FeO-rich chondrules and their rims from CR chondrites. 26th Goldschmidt Conference (abstract).

Nakamura T., Noguchi T., Tsuchiyama A., Ushikubo T., Kita N. T., Valley J. W., Zolensky M. E., Kakazu Y., Sakamoto K., Mashio E., Uesugi K., and Nakano T. (2008) Chondrulelike objects in short-period comet 81P/Wild 2. *Science* **321**, 1664–1667.

Nakamura T., Noguchi T., Tanaka M., Zolensky M. E., Kimura M., Tsuchiyama A., Nakato A., Ogami T., Ishida H., Uesugi M., Yada T., Shirai K., Fujimura A., Okazaki R., Sandford S. A., Ishibashi Y., Abe M., Okada T., Ueno M., Mukai T., Yoshikawa M., and Kawaguchi J. (2011) Itokawa dust particles: A direct link between S-type asteroids and ordinary chondrites. *Science* **333**, 1113–1116.

Nakashima D., Ushikubo T., Joswiak D. J., Brownlee D. E., Matrajt G., Weisberg M. K., Zolensky M. E., and Kita N. T. (2012) Oxygen isotopes in crystalline silicates of comet Wild 2: A comparison of oxygen isotope systematics between Wild 2 particles and chondritic materials. *Earth Planet. Sc. Lett.* **357-358**, 355–365.

Nakashima D., Ushikubo T., Kita N. T., Weisberg M. K., Zolensky M. E., and Ebel D. S. (2015) Late formation of a comet Wild 2 crystalline silicate particle, Pyxie, inferred from Al-Mg chronology of plagioclase. *Earth Planet. Sc. Lett.* **410**, 54–61.

Nguyen A. N., Berger E. L., Nakamura-Messenger K., Messenger S., and Keller L. P. (2017) Coordinated mineralogical and isotopic analyses of a cosmic symplectite discovered in a comet 81P/Wild 2 sample. *Meteorit. Planet. Sci.* **52**, 2004–2016.

Ogliore R. C., Huss G.R., Nagashima K., Butterworth A. L., Gainsforth Z., Stodolna J., Westphal A. J., Joswiak D., and Tyliszczak T. (2012) Incorporation of a late-forming chondrule into comet Wild 2. *Astrophys. J. Lett.* **745**, L19 (5pp).

Ogliore R. C., Nagashima K., Huss G. R., Westphal A. J., Gainsforth Z., and Butterworth A. L. (2015) Oxygen isotopic composition of coarse- and fine-grained material from comet 81P/Wild 2. *Geochim. Cosmochim. Acta* **166**, 74–91.

Ormel C. W., Spaans M., and Tielens A. G. G. M. (2007) Dust coagulation in protoplanetary disks: Porosity matters. *Astron. Astrophys.* **461**, 215–232.

Poppe, T., Blum, J., and Henning, T. (2000) Analogous experiments on the stickiness of micron-sized preplanetary dust. *Astrophys. J.* **533**, 454–471.

Poppe T. and Schräpler R. (2005) Further experiments on collisional tribocharging of cosmic grains. *Astron. Astrophys.* **438**, 1–9.

Royer J. R., Evans D. J., Oyarte L., Guo Q., Kapit E., Möbius M. E., Waitukaitus S. R., and Jaeger H. M. (2009) High-speed tracking of rupture and clustering in freely falling granular streams. *Nature* **459**, 1110–1113.

Rubin A. E. (2010) Physical properties of chondrules in different chondrite groups: Implications for multiple melting events in dusty environments. *Geochim. Cosmochim. Acta* **74**, 4807–4828.

Ruzicka A., Floss C., and Hutson M. (2012) Agglomeratic olivine (AO) objects and type II chondrules in ordinary chondrules: Accretion and melting of dust to form ferroan chondrules. *Geochim. Cosmochim. Acta* **76**, 103–124.

Schrader D. L., Franchi I. A., Connolly H. C. Jr., Greenwood R. C., Lauretta D. S., and Gibson J. M. (2011) The formation and alteration of the Renazzo-like carbonaceous chondrites I: Implications of bulk-oxygen isotopic composition. *Geochim. Cosmochim. Acta* **75**, 308–325.

Schrader D. L., Connolly H. C. Jr., Lauretta D. S., Nagashima K., Huss G. R., Davidson J., and Domanik K. J. (2013) The formation and alteration of the Renazzo-like carbonaceous chondrites II: Linking O-isotope composition and oxidation state of chondrule olivine. *Geochim. Cosmochim. Acta* **101**, 302–327.

Schrader D. L., Nagashima K., Krot A. N., Ogliore R. C., and Hellebrand E. (2014) Variations in the O-isotope compositions of gas during the formation of chondrules from the CR chondrites. *Geochim. Cosmochim. Acta*. **132**, 50–74.

Schrader D. L., Connolly H. C. Jr., Lauretta D. S., Zega T.J., Davidson J., and Domanik K. J. (2015) The formation and alteration of the Renazzo-like carbonaceous chondrites III: Toward understanding the genesis of ferromagnesian chondrules. *Meteorit. Planet. Sci.* **50**, 15–50.

Schrader D. L., Nagashima K., Krot A. N., Ogliore R. C., Yin Q.-Z., Amelin Y. A., Stirling C. H., and Kaltenbach A. (2017) Distribution of ^{26}Al in the CR chondrite chondrule-forming region of the protoplanetary disk. *Geochim. Cosmochim. Acta*. **201**, 275–302.

Shu F. H., Shang H., and Lee T. (1996) Toward an astrophysical theory of chondrites. *Science* **271**, 1545–1552.

Skrutskie M. F., Dutkevitch D., Strom S. E., Edwards S., Strom K. M., and Shure M. A. (1990) A sensitive 10 μm search for emission arising from circumstellar dust associated with solar-type pre-main-sequence stars. *Astron. J.* **99**, 1187–1195.

Su K. Y. L, De Buizer J. M., Rieke G. H., Krinov A. V., Löhne T., Marengo M., Stapelfeldt K. R., Ballering N. P., and Vacca W. D. (2017). The inner 25 au debris distribution in the ε Eri system. *Astron. J.* **153**, 226–237.

Sugiura N. and Fujiya W. (2014) Correlated accretion ages and ε^{54}Cr of meteorite parent bodies and the evolution of the solar nebula. *Meteorit. Planet. Sci.* **49**, 772–787.

Tenner T. J., Nakashima D., Ushikubo T., Kita N. T., and Weisberg M. K. (2015) Oxygen isotope ratios of FeO-poor chondrules in CR3 chondrites: Influence of dust enrichment and H_2O during chondrule formation. *Geochim. Cosmochim. Acta* **148**, 228–250.

Ushikubo T., Kimura M., Kita N. T., and Valley J. W. (2012) Primordial oxygen isotope reservoirs of the solar nebula recorded in chondrules in Acfer 094 carbonaceous chondrite. *Geochim. Cosmochim. Acta* **90**, 242–264.

Van Kooten E. M. M. E., Wielandt D., Schiller M., Nagashima K., Thomen A., Larsen K. K., Olsen M. B., Nordlund K., Krot A. N., and Bizzarro M. (2016) Isotopic evidence for primordial molecular cloud material in metal-rich carbonaceous chondrites. Proc. *Natl. Acad. Sci.* **113**, 2011–2016.

Villeneuve J., Chaussidon M., and Libourel G. (2009) Homogeneous distribution of ^{26}Al in the solar system from the Mg isotopic composition of chondrules. *Science* **325**, 985–988.

Waitukaitis S. R. and Jaeger H. M. (2013) In situ granular charge measurement by free-fall videography. *Rev. Sci. Instrum.* **84**, 025104–10.

Waitukaitis S. R., Lee V., Pierson J. M., Forman S. L., and Jaeger H. M. (2014) Size-Dependent same-material tribocharging in insulating grains. *Phys. Rev. Lett.* **112**, 218001–5.

Walsh K. J., Morbidelli A., Raymond S. N., O'Brien D. P., and Mandell A. M. (2011) A low mass for Mars from Jupiter's early gas-driven migration. *Nature* **475**, 206–209.

Warren P. H. (2011) Stable-isotopic anomalies and the accretionary assemblage of the Earth and Mars: A subordinate role for carbonaceous chondrites. *Earth Planet. Sci. Lett.* **311**, 93–100.

Weisberg M. K. and Prinz M. (1994) Agglomeratic olivine chondrules. *Lunar Planet. Sci. XXV*. Lunar Planet. Inst., Houston, pp. 1481–1482 (abstr.).

Weisberg M. K. and Prinz M. (1996) Agglomeratic chondrules, chondrule precursors, and incomplete melting. In Chondrules and the Protoplanetary Disk (eds. R. H. Hewins, R. Jones and E. Scott). pp. 119–128.

Weisberg M. K., Connolly H. C. Jr., and Ebel D. S. (2004) Petrology and origin of amoeboid olivine aggregates in CR chondrites. *Meteorit. Planet. Sci.* **39**, 1741–1753.

Westphal A. J., Bridges J. C., Brownlee D. E., Butterworth A. L., DeGregorio B. T., Dominguez G., Flynn G. J., Gainsforth Z., Ishii H. A., Jowiak D., Nittler L. R., Ogliore R. C., Palma R., Pepin R. O., Stephan T., and Zolensky M. E. (2017) The future of Stardust science. *Meteorit. Planet. Sci.* **52**, 1859–1898.

Williams J. P. and Cieza L. A. (2011) Protoplanetary disks and their evolution. *Ann. Rev. Astron. Astr.* **49**, 67-117.

Wooden D. H., Ishii H. A., and Zolensky M. E. (2017) Cometary dust: the diversity of primitive refractory grains. *Phil. Trans. R. Soc. A* **375**, 20160260.

Yurimoto H. and Wasson J. T. (2002) Extremely rapid cooling of a carbonaceous-chondrite chondrule containing very ^{16}O-rich olivine and a ^{26}Mg-excess. *Geochim. Cosmochim. Acta* **66**, 4355–4363.

Zolensky M. E., Zega T. J., Yano H., Wirick S., Westphal A. J., Weisberg M. K., Weber I., Warren J. L., Velbel M. A., Tsuchiyama A., Tsou P., Toppani A., Tomioka N., Tomeoka K., Teslich N., Taheri M., Susini J., Stroud R., Stephan T., Stadermann F. J., Snead C. J., Simon S. B., Simionovici A., See T. H., Robert F., Rietmeijer F. J. M., Rao W., Perronnet M. C., Papanastassiou D. A., Okudaira K., Ohsumi K., Ohnishi I., Nakamura-Messenger K., Nakamura T., Mostefaoui S., Mikouchi T., Meibom A., Matrajt G., Marcus M. A., Leroux H., Lemelle L., Le L., Lanzirotti A., Langenhorst F., Krot A. N., Keller L. P., Kearsley A. T., Joswiak D., Jacob D., Ishii H., Harvey R., Hagiya K., Grossman L., Grossman J. N., Graham G. A., Gounelle M., Gillet P., Genge M. J., Flynn G., Ferroir T., Fallon S., Ebel D. S., Dai Z. R., Cordier P., Clark B., Chi M. F., Butterworth A. L., Brownlee D. E., Bridges J. C., Brennan S., Brearley A., Bradley J. P., Bleuet P., Bland P. A., and Bastien R. (2006) Mineralogy and petrology of comet 81P/Wild 2 nucleus samples. *Science* **314**, 1735–1739.

Schrader D. L., Nagashima K., Waitukaitis S. R., Davidson J., McCoy T. J., Connolly Jr. H. C., and Lauretta D. S. (2018) The retention of dust in protoplanetary disks: Evidence from agglomeratic olivine chondrules from the outer Solar System. *Geochim. Cosmochim. Acta.* **223**, 405–421.

TABLES

Table 1. Agglomeratic olivine chondrule summary

Meteorite	Chondrule	Type[1]	Texture[2]	Size (mm)[3]	Fa[4]	Chemical Analyses Fe/Mn	Chemical Analyses # Analyses	O-isotope Analyses $\Delta^{17}O$ (‰)	O-isotope Analyses # Analyses	Reference[5]
EET 92048,7	AO1	AO/II	AO/POP-comp	0.56–1.73	7.7–38.4	27–80	19	none	none	a
Gao-Guenie (b) UA2301,1	Ch14	AO/II	AO/POP-comp	0.22–0.30	1.6–41.7	18–116	15	−24.3 to −1.6	4	a
Gao-Guenie (b) UA2301,1	Ch18	AO/II	AO/POP-comp	0.22–0.37	3.6–54.5	22–115	20	−12.0 to −1.4	5	a
Gao-Guenie (b) UA2301,1	Ch21	AO/II	AO/PO-comp	0.06–0.26	26.6–36.1	52–67	12	0.2 to 0.4	2	a
Gao-Guenie (b) UA2301,1	Ch21B	AO	AO	0.13–0.17	16.8–37.6	37–49	9	−24.6 to −1.8	2	a
Gao-Guenie (b) UA2301,1	Ch22	AO	AO	0.05–0.08	4.5–36.4	14–51	9	−25.4 to −0.7	2	a
GRA 95229,22	Ch15	AO	AO	0.94–1.01	0.8–12.5	3–15	4	−6.8 to −2.1	2	b
PCA 91082,15	AO1	AO	AO	0.17–0.60	5.5–36.7	19–76	20	−6.4 to −0.5	4	a

[1]AO = agglomeratic olivine chondrule; II = type II chondrule.
[2]comp = compound chondrule; PO = porphyritic olivine; POP = porphyritic olivine pyroxene.
[3]Size (mm): minimum–maximum apparent diameter.
[4]Fa = fayalite number.
[5] a = this study. b = Schrader et al. (2013).

Table 2. O-isotope analyses of AO chondrules.

Meteorite	Ch[1]	Type[2]	Grain	Analysis #	Grain Setting[3]	EPMA #[4]	Fa[5]	$\delta^{18}O$	2σ	$\delta^{17}O$	2σ	$\Delta^{17}O$	2σ	Reference[6]
Gao-Guenie (b) UA2301,1	Ch14	AO/POP-comp	G6	Ch14-1	II	106	29.1	-3.1	1.1	-5.7	1.8	-4.1	1.9	a
Gao-Guenie (b) UA2301,1	Ch14	AO/POP-comp	G6	Ch14-2	II	105	24.0	-5.1	1.2	-5.5	1.9	-2.8	2.0	a
Gao-Guenie (b) UA2301,1	Ch14	AO/POP-comp	G8	Ch14-3	AO	110	41.7	-3.6	1.2	-3.5	2.1	-1.6	2.1	a
Gao-Guenie (b) UA2301,1	Ch14	AO/POP-comp	G7	Ch14-4	AO	108	1.6	-51.8	1.2	-51.2	2.1	-24.3	2.2	a
Gao-Guenie (b) UA2301,1	Ch18	AO/POP-comp	G1	Ch18-1	II	146	18.8	1.2	1.2	-1.4	2.0	-2.0	2.1	a
Gao-Guenie (b) UA2301,1	Ch18	AO/POP-comp	G1	Ch18-2	II	148	31.1	0.2	1.3	-1.4	2.0	-1.5	2.1	a
Gao-Guenie (b) UA2301,1	Ch18	AO/POP-comp	G6	Ch18-3	II	158	45.5	-1.4	1.2	-2.1	2.0	-1.4	2.1	a
Gao-Guenie (b) UA2301,1	Ch18	AO/POP-comp	G4	Ch18-4	AO	153	5.3	-11.5	1.2	-12.2	2.0	-6.2	2.1	a
Gao-Guenie (b) UA2301,1	Ch18	AO/POP-comp	G7	Ch18-5	AO	504	54.5	-28.3	2.7	-26.7	4.1	-12.0	4.4	a
Gao-Guenie (b) UA2301,1	Ch21	AO/PO-comp	G5	Ch21-4	II	185	32.2	-1.2	1.2	-0.2	2.1	0.4	2.2	a
Gao-Guenie (b) UA2301,1	Ch21	AO/PO-comp	G1	Ch21-5	II	178	31.5	-3.9	1.6	-1.8	1.8	0.2	2.0	a
Gao-Guenie (b) UA2301,1	Ch21B	AO	G9	Ch21B-2	AO	192	17.8	-51.3	1.3	-51.3	1.9	-24.6	2.0	a
Gao-Guenie (b) UA2301,1	Ch21B	AO	G9	Ch21B-3	AO	519	34.9	-3.7	2.1	-3.7	2.4	-1.8	2.6	a
Gao-Guenie (b) UA2301,1	Ch22	AO	G2	Ch22-1	AO	532	31.2	-5.2	1.5	-3.4	2.0	-0.7	2.1	a
Gao-Guenie (b) UA2301,1	Ch22	AO	G1	Ch22-2	AO	318	4.5	-58.0	1.6	-55.6	2.1	-25.4	2.2	a
GRA 95229,22	Ch15	AO	G1	Ch15-6	AO	327	0.8	-5.5	0.4	-9.6	0.6	-6.8	0.6	b
GRA 95229,22	Ch15	AO	G3	Ch15-5	AO	332	2.8	3.0	0.5	-0.5	0.5	-2.1	0.6	b
PCA 91082,15	AO1	AO	G7	AO1-1	AO	106	33.3	-5.7	1.2	-5.8	2.1	-2.9	2.2	a
PCA 91082,15	AO1	AO	G17	AO1-2	AO	120	33.0	-10.7	1.2	-12.0	1.9	-6.4	2.0	a
PCA 91082,15	AO1	AO	G28	AO1-3	AO	135	34.2	0.3	1.3	-0.3	2.0	-0.5	2.1	a
PCA 91082,15	AO1	AO	G26	AO1-4	AO	501	36.7	1.4	1.3	-0.3	1.8	-1.1	1.9	a

[1]Ch = chondrule.
[2]AO = agglomeratic olivine chondrule; comp = compound chondrule; PO = porphyritic olivine; POP = porphyritic olivine pyroxene.
[3]Grain Setting: The chondrule morphology the grain is set in: either identical to type II chondrules (II), or fine-grained AO chondrule material.
[4]EPMA # corresponds to data in EA-1.
[5]Fa = fayalite number.
[6]a = this study. b = Schrader et al. (2013).
Analytical conditions; contrast aperture: 400 μm; field aperture: 3000x3000 μm^2; entrance slit: 69 μm; exit slit for mono EM (^{17}O): 172 μm; exit slits for multi FC (^{16}O) and multi EM (^{18}O): 500 μm

FIGURES

Figure 1

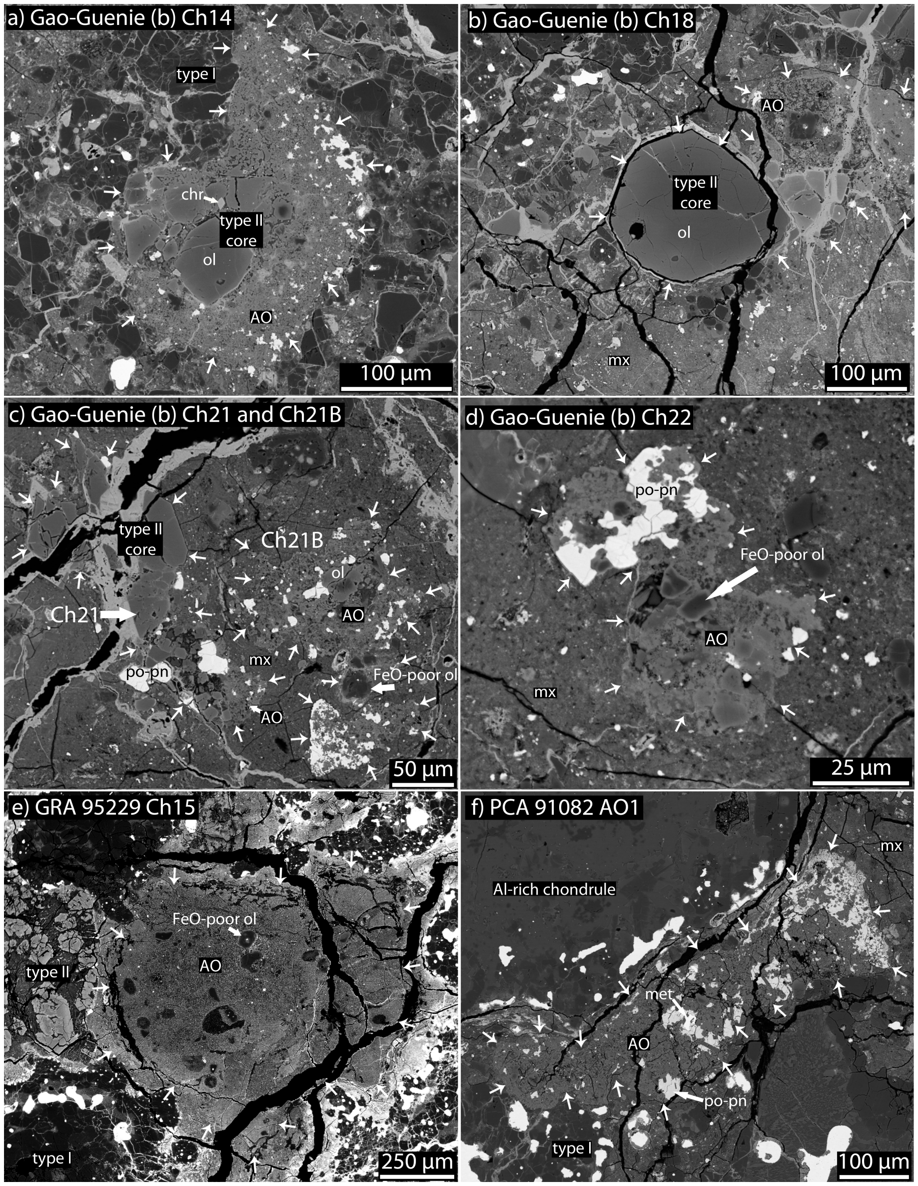

Figure 1. BSE images of agglomeratic-olivine (AO) and AO/type II chondrules with O-isotope data, where arrows not accompanied by phase abbreviations mark the delineation between the AO chondrules and surrounding phases (arrows point toward the AO chondrules). (a) Gao-Guenie (b) Ch14. (b) Gao-Guenie (b) Ch18. (c) Gao-Guenie (b) Ch21 and 21B. (d) Gao-Guenie (b) Ch22. (e) GRA 95229 Ch15, and (f) PCA 91082 AO1. (a–c) show AO/type II chondrules where fine-grained AO material surrounds type II olivine cores (with the exception of Ch21B in part [c]). Ch = chondrule, AO =

agglomeratic olivine texture, ol = olivine, po=pyrrhotite, pn = pentlandite, met = Fe,Ni metal, mx = matrix, type I = type I chondrule, type II = type II chondrule, and chr = chromite. Images of EET 92048 AO1 and SIMS pit locations for all chondrules are in EA-1. Bright veins in Fig. 1a–c result from terrestrial weathering. See EA-1 for higher resolution images.

Figure 2

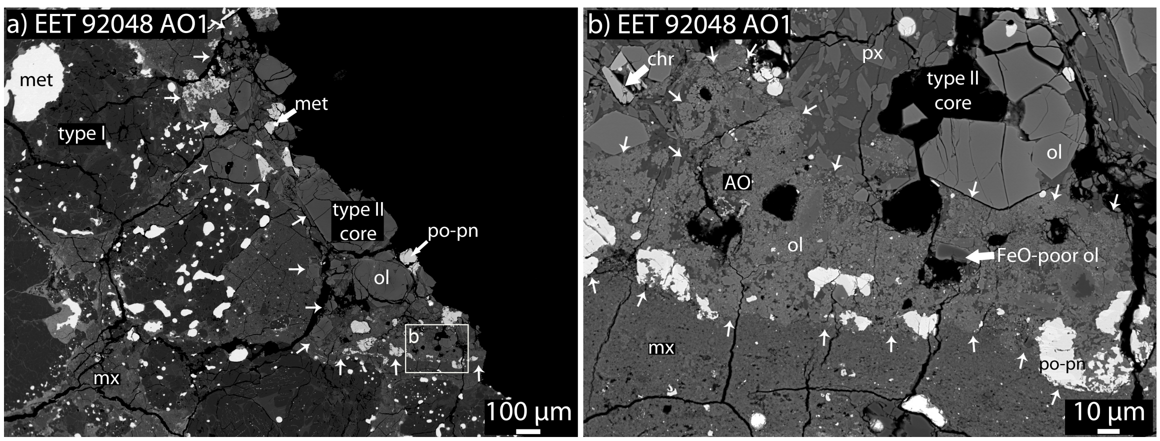

Figure 2. Agglomeratic olivine/type II chondrule in EET 92048. (a) Entire chondrule, where arrows not accompanied by phase abbreviations mark the delineation between the chondrule and surrounding phases. (b) Relatively magnified view of chondrule showing interface between fine-grained AO portion of chondrule (arrows point toward the AO portion) and adjacent type II core and matrix (mx). Where px = pyroxene; see Fig. 1 for other abbreviations. See EA-1 for additional images.

Figure 3

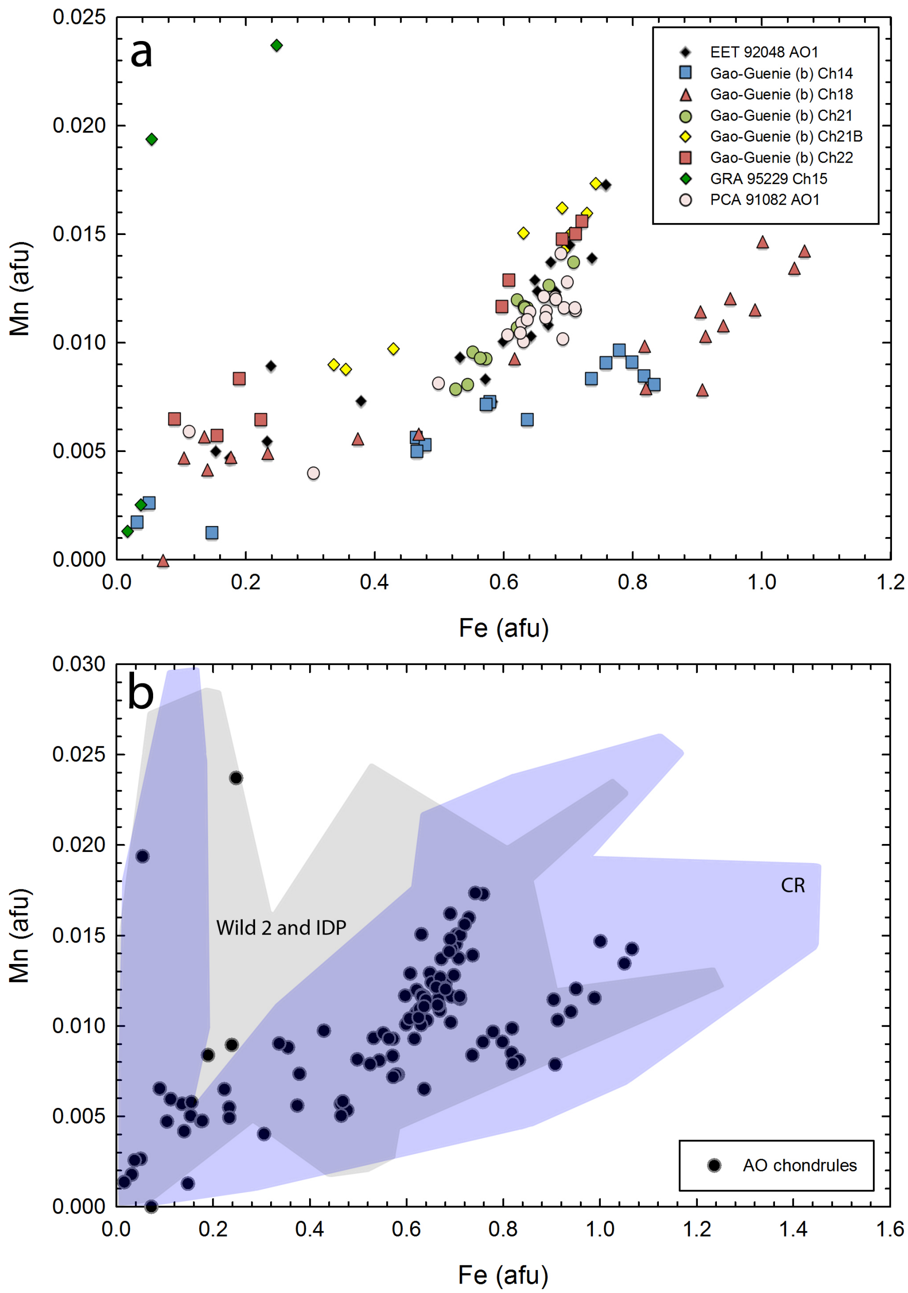

Figure 3. (a) Fe vs. Mn (afu) for FeO-poor and FeO-rich olivine in AO chondrules. (b) Fe vs. Mn (afu) of olivine in AO chondrules compared to FeO-poor and FeO-rich olivine from type I (Fe <0.2) and type II (Fe>0.2) chondrule from CR chondrites (Schrader et al., 2015) and olivine from comet Wild 2 (Frank et al., 2014; Brownlee and Joswiak, 2017) and interplanetary dust particles (IDP; Brownlee and Joswiak, 2017). All *in situ* chemical analyses are in EA-2, and additional chemical plots are in EA-3.

Figure 4

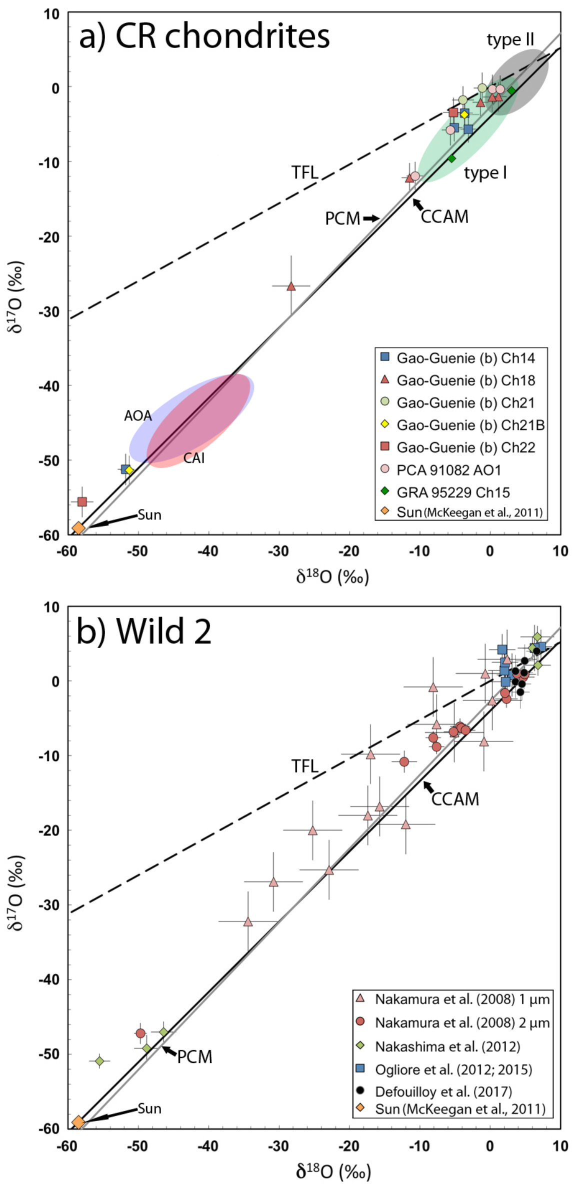

Figure 4. (a) $\delta^{18}O$ vs. $\delta^{17}O$ (‰) for AO chondrules from CR chondrites in this study. GRA 95229 Ch15 is from Schrader et al. (2013). Compositional fields from individual mineral analyses for CR type I and type II chondrules from UH SIMS (Schrader et al., 2013; 2014; 2017), CR amoeboid olivine aggregates (AOA; Aléon et al., 2002) and unaltered calcium-aluminum-rich inclusions (CAI; Makide et al., 2009). O-isotope composition of the Sun ($\delta^{18}O = -58.5‰$, $\delta^{17}O = -59.1‰$) from McKeegan et al. (2011). The O-isotope compositions of olivine from AOs are similar to those from type I and type II chondrules, and ^{16}O-rich olivine is similar to that in AOAs. (b) The O-isotope

compositions of olivine from Wild 2 [Nakamura et al., 2008 (data for 1 and 2 μm spot sizes); Nakashima et al., 2012; Ogliore et al., 2012; 2015; Defouilloy et al., 2017] show a similar compositional range to those of AO chondrules (a). Terrestrial fractionation (TF) line, primitive chondrules minerals (PCM) line from Ushikubo et al. (2012), and carbonaceous chondrite anhydrous mineral (CCAM) line from Clayton et al. (1977) plotted for reference.

Figure 5

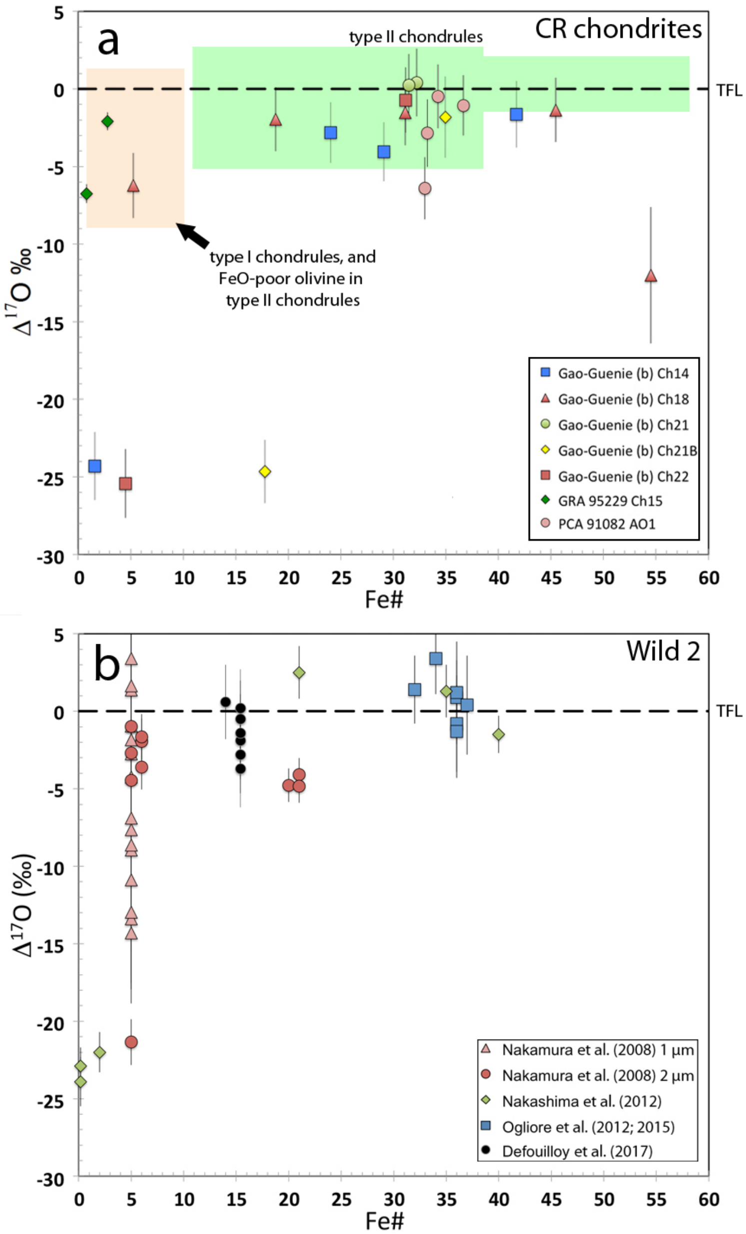

Figure 5. In situ Fe# (Fe/(Fe + Mg)×100) vs. $\Delta^{17}O$ of olivine in (a) AO chondrules compared to fields for type I and type II chondrules from CR chondrites (Schrader et al., 2013; 2014; 2017) and (b) olivine from Wild 2 [Nakamura et al., 2008 (data for 1 and 2 μm spot sizes); Nakashima et al., 2012; Ogliore et al., 2012; 2015; Defouilloy et al., 2017]. Data from GRA 95229 Ch15 in (a) from Schrader et al. (2013). Terrestrial fractionation (TF) line plotted for reference.

ELECTRONIC ANNEXES

EA-1: All BSE images with SIMS pits marked.

EA-2: All silicate data.

EA-3: Plots of FeO vs. CaO, Cr_2O_3, and MnO of AO chondrule olivine, and comparisons to type I and type II chondrules from CR chondrites.